Inorganic Chemistry

Article

pubs.acs.org/IC

Turning on Single-Molecule Magnet Behavior in a Linear $\{Mn_3\}$ Compound

Fatemah Habib,[†] Gabriel Brunet,[†] Francis Loiseau,[†] Thushan Pathmalingam,[†] Tara J. Burchell,[†] André M. Beauchemin,[†,‡] Wolfgang Wernsdorfer,[§] Rodolphe Clérac,*[,∥,⊥] and Muralee Murugesu*[,†,‡]

[†]Department of Chemistry, University of Ottawa, 10 Marie-Curie, Ottawa, Canada K1N6N5

[‡]Centre for Catalysis Research and Innovation, 30 Marie-Curie, Ottawa, Canada

[§]Institut Néel, CNRS and Université Joseph Fournier, BP 166, 25 Avenue des Martyrs, 38042 Grenoble Cedex 9, France

[∥]CNRS, CRPP, UPR 8641, F-33600 Pessac, France

[⊥]Univ. Bordeaux, CRPP, UPR 8641, F-33600 Pessac, France

Supporting Information

ABSTRACT: The synthesis, structure, and magnetic properties are reported for a new manganese compound with a mixed-valent $\{Mn_3\}$ core arranged in a linear fashion. The previously reported complex **1**, $[Mn^{IV}_3(dpo)_6]\cdot 2MeCN$, where H_2dpo is (*E*)-1-hydroxy-1,1-diphenylpropan-2-one oxime, served as a starting point for the isolation of a $\{Mn_3\}$ compound with an analogous core arrangement through the reaction of $Mn(OAc)_2\cdot 4H_2O$, H_3oxol ((*E*)-2,5-dihydroxy-2,5-dimethylhexan-3-one oxime), and NaOH in MeOH and MeCN. By using these reaction conditions, compound **2**, $Na[Mn^{IV}_2Mn^{III}(Hoxol)_6]_n\cdot MeOH\cdot H_2O$, was successfully isolated revealing a central Mn^{III} ion thereby introducing structural and magnetic anisotropy to the system. The structure of **2** reveals linear trinuclear $Mn^{IV}-Mn^{III}-Mn^{IV}$ units connected through Na^+ ions forming a linear one-dimensional coordination polymer. The Jahn–Teller axes of each trinuclear unit are aligned parallel within the same chain and form a 75° angle between the two symmetry related chains. Magnetic susceptibility measurements of **1** and **2** in the temperature range 1.9–300 K reveal that only the reduced compound, **2**, is a single-molecule magnet (SMM) largely due to the anisotropy introduced by the Jahn–Teller distortions on the Mn^{III} ions, which effectively induce this magnet behavior. Weak antiferromagnetic interactions along the chains through the Na^+ cations lead to a modulation of the intrinsic properties of the $Mn^{IV}-Mn^{III}-Mn^{IV}$ SMMs.

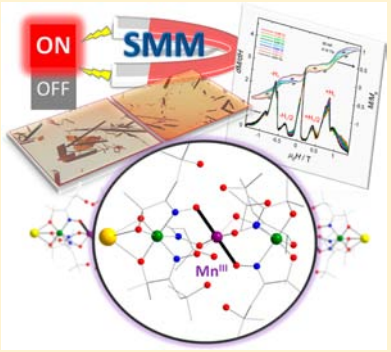

INTRODUCTION

In recent years, metal oxime chemistry has become an intense research focus in the field of molecular magnetism as they provide systems, which can be methodically fine-tuned to form single-molecule magnets (SMMs), with applications as high density storage materials and quantum computing.[1] Lately, it has been demonstrated that ferromagnetic interactions can be promoted between Mn^{III} ions via oximate ligands.[1b,c] In the reported oximate-based $\{Mn_3\}$ and $\{Mn_6\}$ complexes, a slight ligand modification has generated a larger Mn–N–O–Mn torsion angle that in turn induced the parallel alignment of the spins.[2] Such a careful systematic approach has led to complexes with large spin ground states (*S*).[3] When large spins are combined with uniaxial Ising-like magnetic anisotropy, slow relaxation of the magnetization can be observed. Molecules with such magnet-like behavior are termed SMMs.[4] To date, the use of tunable oxime ligands has led to the largest energy barrier for a 3*d* metal ion based SMM.[5] However, more research is necessary to induce and control magnetic anisotropy for obtaining complexes with even larger energy barriers. One approach is to incorporate highly anisotropic lanthanide ions in transition-metal complexes in order to increase the Ising-type anisotropy, thereby obtaining SMMs with higher barriers.[6] Another, more methodical, approach is to modify high-spin complexes to induce anisotropy by controlling the oxidation states of the metal centers. The former strategy has been shown to yield SMMs with larger energy barriers,[7] whereas the latter remains quite challenging and is being actively pursued, since a certain degree of control over structural distortions is highly desirable.

In manganese chemistry, magnetic anisotropy can be obtained through the isolation of complexes with Mn^{III} ions where the magnetic anisotropy arises from the observed Jahn–Teller (J–T) distortions.[8] The spin vector naturally aligns along one axis, known as the easy axis, and that corresponds to the Mn^{III} J–T axis. In such molecules, controlled isolation of Mn^{III} ions in order to increase the Ising-type anisotropy is difficult as often mixed $Mn^{II}/Mn^{III}/Mn^{IV}$ oxidation states are encountered in these complexes.[9] With this in mind, our aim is to induce magnetic anisotropy in a known high-spin manganese complex by simply stabilizing Mn ions with a +3 oxidation state, while

Received: August 20, 2012
Published: January 23, 2013

   dx.doi.org/10.1021/ic301820w | *Inorg. Chem.* 2013, 52, 1296–1303

increasing the spin ground state of the complex simultaneously. We have recently reported a linear Mn^{IV}_3 complex, $[Mn^{IV}_3(dpo)_6]\cdot 2MeCN$, **1**, where H_2dpo is (*E*)-1-hydroxy-1,1-diphenylpropan-2-one oxime (Scheme 1), bridged solely by

Scheme 1[a]

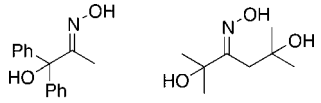

[a] H_2dpo: (*E*)-1-hydroxy-1,1-diphenylpropan-2-one oxime. H_3oxol: (*E*)-2,5-dihydroxy-2,5-dimethylhexan-3-one oxime.

oxime ligands with an $S = {}^9/_2$ spin ground state.[10] Our initial studies along with electrochemical experiments indicated that the central Mn^{IV} ion in the trinuclear complex can be reduced to Mn^{III} thus inducing magnetic anisotropy. Consequently, our synthetic strategy consisted of employing similar oxime chelating ligands in order to retain the same superexchange pathway between the metal centers, thus giving a way to a comparable structural core. Initial tests revealed that the addition of reducing agents resulted in rapid decomposition of the metal complex. Other means of reducing the central Mn^{IV} ion, such as cyclic voltammetry, were investigated; however, no trinuclear complex could be isolated. Herein, we report the synthesis, structure, and magnetic properties of an analogous linear $\{Mn_3\}$ compound, $Na[Mn^{IV}_2Mn^{III}(Hoxol)_6]_n\cdot MeOH\cdot H_2O$, **2**, where H_3oxol is the (*E*)-2,5-dihydroxy-2,5-dimethylhexan-3-one oxime ligand (Scheme 1), with a central Mn^{III} ion. Our strategy proved successful in inducing magnetic anisotropy in an oxime bridged linear high-spin manganese unit.

EXPERIMENTAL SECTION

General Considerations. All chemical reagents and solvents used in these syntheses were obtained commercially and without further purification. "***Caution!*** *Due to the high energy content of* NH_2OH*, appropriate care should be taken when conducting these experiments. The hydroxylamine concentration should not be increased beyond 5−10 wt % (i.e., the typical reaction conditions), and appropriate safety controls should be performed before scaling up this chemistry above the gram scale, especially at very high temperatures.*"

Synthesis of (*E*)-1-Hydroxy-1,1-diphenylpropan-2-one Oxime (H_2dpo). An oven-dried microwave tube (10 mL), equipped with a magnetic stir bar and a rubber septum, was purged with an argon balloon for 5 min. 1,1-Diphenylprop-2-yn-1-ol (1.25 g, 6.00 mmol), aqueous hydroxylamine (920 μL of a 50 wt % solution, 15.0 mmol), and isopropanol (freshly distilled, 6 mL) were added to the reaction vessel while keeping a constant flow of argon. The rubber septum was quickly replaced by a microwave aluminum cap. The mixture was heated in a CEM microwave for 4 h at 140 °C. After cooling the mixture to room temperature, the crude was concentrated under reduced pressure and purified through column chromatography (7.5% EtOAc in toluene). The H_2dpo ligand was isolated as a white powder (1.05 g, 78% yield); H^1 NMR (DMSO-d_6, 300 MHz) δ 10.90 (s, 1H), 7.31−7.30 (m, 8H), 7.28−7.18 (m, 2H), 6.41 (s, 1H), 1.81 (s, 3H); ^{13}C NMR (DMSO-d_6, 75 MHz) δ 159.6, 145.1, 127.4, 127.3, 126.5, 80.9, 12.0; IR (film, cm^{-1}): 3332, 1659, 1602, 1488, 1443, 1374, 1051, 1013, 968, 880, 758, 728, 694; HRMS (EI): exact mass calculated for $C_{15}H_{14}NO^+[M - OH]^+$: 224.1070; found: 224.1053.

Synthesis of (*E*)-2,5-Dihydroxy-2,5-dimethylhexan-3-one Oxime (H_3oxol). 2,5-Dimethylhex-3-yne-2,5-diol (4.27 g, 30.0 mmol), aqueous hydroxylamine (2.76 mL of a 50 wt % solution, 45.1 mmol), and isopropanol (freshly distilled, 30 mL) were added to a sealed tube. The mixture was heated in a wax bath for 24 h at 100 °C. After cooling to room temperature, the mixture was concentrated under reduced pressure and recrystallized from hot hexanes. The H_3oxol ligand was isolated as white powder (2.89 g, 55% yield); H^1 NMR (DMSO-d_6, 300 MHz) δ 10.55 (s, 1H), 5.67 (s, 1H), 5.48 (s, 1H), 2.63 (s, 2H), 1.29 (s, 6H), 1.17 (s, 6H); ^{13}C NMR (DMSO-d_6, 75 MHz) δ 161.9, 71.9, 70.3, 36.9, 30.7, 29.9; IR (film, cm^{-1}) 3423, 2970, 1674, 1601, 1464, 1355, 1179, 1153, 1114, 1042, 963, 895, 864, 672, 612; HRMS (EI): exact mass calculated for $C_8H_{16}NO_2^+[M - OH]^+$: 158.1181; found: 158.1200.

Preparation of $[Mn^{IV}_3(H_2dpo)_6]\cdot 2MeCN$ (1). The reaction of $Mn(ClO_4)_2\cdot 6H_2O$ (0.25 mmol, 0.091 g) with H_2dpo (0.5 mmol, 0.121 g) and Et_3N (0.25 mmol, 0.035 mL) in 10:10 mL of MeOH/MeCN gave a dark-brown opaque solution. The filtrate was left undisturbed for a period of 4 days, after which, dark-brown rectangular crystals suitable for X-ray crystallography were isolated in 45% yield with respect to Mn. Selected IR (KBr pellet, cm^{-1}): 3451 (br), 3074 (m), 1600 (m), 1501 (m), 1450 (m), 1077 (m), 1026 (s), 1000 (s), 949 (m), 916 (w), 775 (w), 750 (w), 705 (s), 690 (s).

Preparation of $Na[Mn^{IV}_2Mn^{III}(Hoxol)_6]_n\cdot(MeOH, H_2O)$ (2). Compound **2** was synthesized by the reaction of $Mn(OAc)_2\cdot 4H_2O$ (0.25 mmol, 0.061 g) with H_3oxol (0.25 mmol, 0.045 g) and NaOH (1.0 mmol, 0.040 g) in 5 mL of MeOH and 10 mL of MeCN giving a dark-brown opaque solution similar to complex **1**. Crystallization of the compound was performed over a period of 1 week to provide dark-brown needle-like crystals suitable for X-ray crystallography with a yield of 64% with respect to Mn. Selected IR (KBr pellet, cm^{-1}): 3440 (br), 2975 (m), 2924 (m), 1605 (w), 1465 (w), 1350 (m), 1155 (s), 1118 (s), 1056 (s), 974 (s), 890 (w), 865 (w). Anal. Calcd for $C_{48}H_{90}Mn_3N_6NaO_{18}$: C, 46.98%; H, 7.41%; N, 6.85%. Found: C, 46.84%; H, 7.35%; N, 6.81%.

Physical Measurements. X-ray crystallographic data were collected on single dark-brown crystals mounted on a glass fiber for complexes **1** and **2** (Figure 1). Unit cell measurements and intensity data collections were performed on a Bruker-AXS SMART 1 k CCD and Bruker APEX II diffractometer for **1** and **2**, respectively, using graphite monochromatized Mo Kα radiation (λ = 0.71073 Å) for **1** and Cu Kα radiation (λ = 1.54178 Å) for **2**. The data reduction included a correction for Lorentz and polarization effects, with an applied multiscan absorption correction (SADABS). The reflection data was consistent with triclinic *P*-1 and monoclinic $P2_1/c$ systems for **1** and **2**, respectively. The crystal structure was solved and refined using the SHELXTL program suite.[19] Direct methods yielded all non-hydrogen atoms that were refined with anisotropic thermal parameters. All hydrogen atom positions were calculated geometrically and were riding on their respective atoms. For compound **2**, the option squeeze was used to correct the data for the presence of disordered solvent molecules (H_2O, MeOH). Crystallographic data for **1** and **2** are presented in Table S1 of the Supporting Information.

IR analyses were obtained by using a Nicolet Nexus 550 FT-IR spectrometer in the 4000−650 cm^{-1} range. The spectra were obtained by preparing KBr pellets.

NMR spectroscopic analyses were conducted on a Bruker Avance 300 MHz spectrometer with a 5 mm autotuning broadband probe with Z gradient.

The magnetic susceptibility measurements were obtained using a Quantum Design superconducting quantum interference device (SQUID) magnetometer MPMS-XL7 that works between 1.8 and 300 K for direct current (dc) applied fields ranging from −7 to 7 T. Measurements were performed on polycrystalline samples of 4.58 mg for **1** and 31.3 mg for **2**. Alternating current (ac) susceptibility measurements were performed under an oscillating ac field of 3 Oe and ac frequencies that ranged from 10 to 1500 Hz. Ferromagnetic impurities that were absent in both samples were investigated by collecting magnetization data at 100 K. All magnetic data were corrected for the sample holder as well as diamagnetic contributions.

dx.doi.org/10.1021/ic301820w | *Inorg. Chem.* 2013, 52, 1296−1303

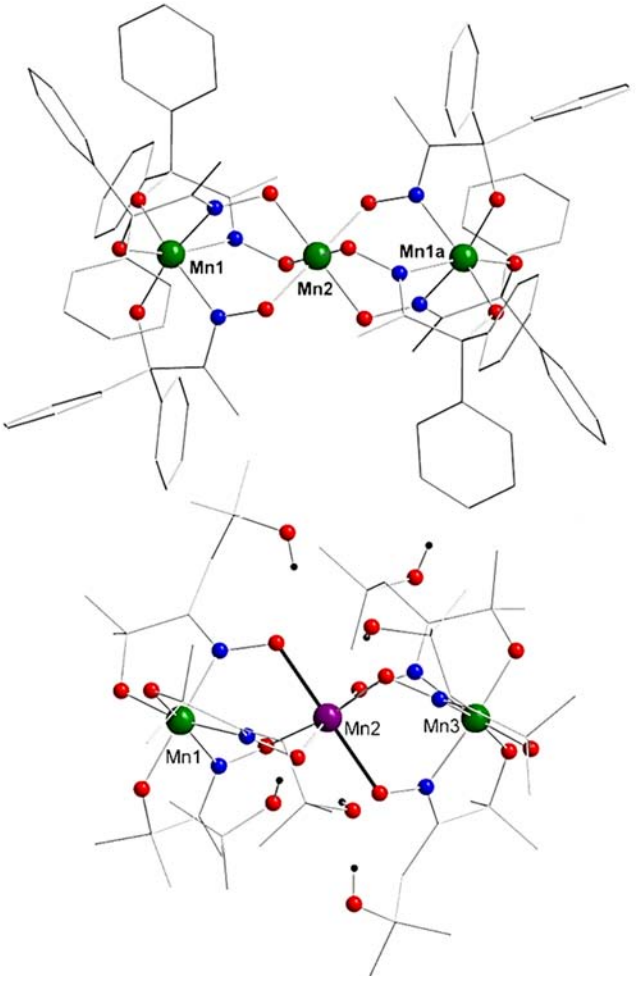

Figure 1. (top) Molecular structure of complex **1**. Symmetry equivalent labels are denoted by an additional "a" in the label (Mn1a). (bottom) Structure of the trinuclear unit in compound **2** revealing the J–T distortion (black bond) on the central Mn atom. Color code: green (Mn^{IV}), purple (Mn^{III}), red (O), blue (N), gray (C), black (H). Most H atoms are omitted for clarity.

RESULTS AND DISCUSSION

Syntheses. Employing polydentate ligands such as H_2dpo and H_3oxol is essential for the synthesis of multinuclear complexes due to their ability to coordinate multiple metal ions simultaneously. The coordination of the ligands to metal ions is promoted by the deprotonation of the hydroxyl and oximate groups by a base, such as NaOH or Et_3N, forming stable five- or six-membered coordination rings. The previously published complex, **1**,[10] was synthesized through the reaction of $Mn(ClO_4)_2$ with H_2dpo and Et_3N in MeOH and MeCN yielding dark-brown rectangular crystals (Figure 1, left). The resulting complex consisted of a trinuclear $\{Mn_3\}$ unit where all Mn ions were in the +4 oxidation state (Figure 1, top). In order to introduce magnetic anisotropy and hence potentially induce SMM behavior, we set out to reduce the central Mn^{IV} ion to Mn^{III} that was shown to be accessible through density functional theory calculations.[10]

Initially, the synthesis of a reduced analogue of **1** consisted of employing a less bulky ligand. This approach would increase the flexibility of the complex and possibly create an opening for potentially distorting the coordination sphere of the central Mn ion leading to elongation/compression of one axis. These attempts included replacing the phenyl groups of H_2dpo with diethyl groups, which did not yield the desired complex. Other strategies included the addition of a moderate strength reducing agent, such as sodium borohydride, which resulted in complex decomposition as well as reduction through cyclic voltammetry. However, the reduced complex could not be isolated preventing further characterization. Consequently, the reaction conditions were varied in terms of ligand, metal ion source, base, and solvent.

Compound **2** was obtained by changing the base from Et_3N to NaOH as well as the metal ion source from $Mn(ClO_4)_2$ to $Mn(OAc)_2$. Crystallization of **2** occurred from the mother liquor in a period of 1 week resulting in small needle-like crystals suitable for single crystal X-ray diffraction. It is noteworthy that an excess of base was used; however, only two hydroxy groups were deprotonated leaving the remaining hydroxy group to form hydrogen bonds within the coordination sphere of the central Mn^{III} ion. Furthermore, the remaining base in the reaction allowed for the slow oxidation of the manganese atoms. Its dual role as a base, as well as a source of the bridging Na^+ ions linking the trinuclear units (Figure 1, bottom; and Figure 2), was confirmed when other potential

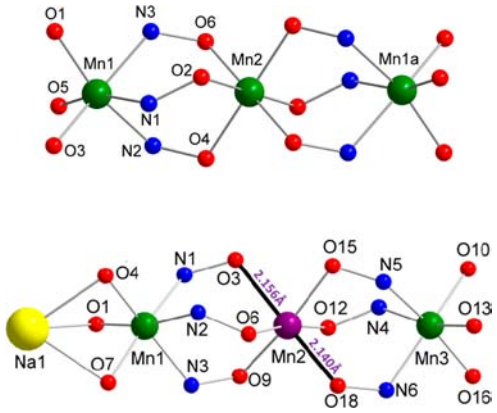

Figure 2. (top) Core structure of the linear trinuclear complex **1** showing the triple oximate superexchange pathways between the manganese centers. (bottom) Core structure of **2** showing the trinuclear unit bridged by Na atoms with the J–T distortion on the central Mn(2) atom indicated in black bonds. Color code: green (Mn^{IV}), purple (Mn^{III}), red (O), blue (N), yellow (Na).

sodium sources, such as sodium chloride, were added but no crystallized product was observed. Moreover, the sodium ions are a key contributing factor in the formation of **2** when forming a stable one-dimensional coordination polymer.

Structural Analysis. The structural analysis of both compounds reveals a trinuclear $\{Mn_3\}$ core with a triple oximate superexchange pathway between the manganese centers as shown in Figures 1 and 2. Complex **1** crystallizes in the triclinic *P*-1 space group while **2** crystallizes in monoclinic $P2_1/c$ space group. Compound **1** exhibits a centrosymmetric geometry in which the three Mn centers are linked solely via oximate groups with a 180° Mn(1)–Mn(2)–Mn(1a) angle while **2**, with the reduction of its central manganese atom (Mn2), is no longer centrosymmetric nor perfectly linear (Figure 3). The angle between the three metal centers, Mn(1)–Mn(2)–Mn(3), was determined to be 177°.

In both complexes **1** and **2**, the Mn oxidation states are confirmed by bond-valence sum (BVS) calculations (Table 1) and charge considerations. Furthermore, in compound **2**, the

dx.doi.org/10.1021/ic301820w | Inorg. Chem. 2013, 52, 1296–1303

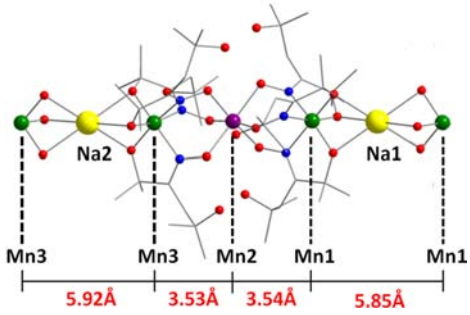

Figure 3. Na ions in **2** linking the trinuclear $\{Mn_3\}$ units forming a one-dimensional structure. Color code: green (Mn^{IV}), purple (Mn^{III}), red (O), blue (N), yellow (Na), gray (C).

Table 1. Bond Valence Sum Calculations with Suggested Oxidation States for 1 and 2

	terminal Mn ion				central Mn2			
compd	Mn^{II}	Mn^{III}	Mn^{IV}	ox state	Mn^{II}	Mn^{III}	Mn^{IV}	ox state
1	4.26	4.00	**4.02**	4	4.03	3.69	**3.87**	4
2	4.36	4.10	**4.13**	4	3.12	**2.85**	2.99	3

oxidation of the central manganese atom from Mn^{II} to Mn^{III} is also confirmed by the elongation of the Mn(2)−O(3) and Mn(2)−O(18) bonds (Table 2) indicating a J−T distortion

Table 2. Selected Bond Distances (Å) and Torsion Angles (deg) for 1 and 2

		Complex **1**	
Mn(1)···Mn(2)	3.54	Mn(1)−N(3)	1.997(9)
Mn(1)···Mn(1a)	7.08	Mn(2)−O(2)	1.911(6)
Mn(1)−O(1)	1.826(7)	Mn(2)−O(4)	1.910(7)
Mn(1)−O(3)	1.834(8)	Mn(2)−O(6)	1.915(6)
Mn(1)−O(5)	1.826(8)	Mn(1)−N(1)−O(2)−Mn(2)	53.5(2)
Mn(1)−N(1)	1.996(8)	Mn(1)−N(2)−O(4)−Mn(2)	51.7(1)
Mn(1)−N(2)	1.989(8)	Mn(1)−N(3)−O(6)−Mn(2)	48.8(2)
		Complex **2**	
Mn(1)···Mn(2)	3.548	Mn(2)−O(18)	2.140(2)
Mn(2)···Mn(3)	3.535	Mn(3)−N(4)	1.981(3)
Mn(1)−O(1)	1.842(2)	Mn(3)−N(5)	1.988(3)
Mn(1)−O(4)	1.847(2)	Mn(3)−N(6)	1.981(3)
Mn(1)−O(7)	1.852(2)	Mn(3)−O(10)	1.852(2)
Mn(1)−N(1)	1.979(3)	Mn(3)−O(13)	1.852(2)
Mn(1)−N(2)	1.977(3)	Mn(3)−O(16)	1.852(2)
Mn(1)−N(3)	1.973(3)	Mn(1)−N(1)−O(3)−Mn(2)	44.7(3)
Mn(2)−O(3)	2.156(2)	Mn(1)−N(2)−O(6)−Mn(2)	48.8(3)
Mn(2)−O(6)	1.964(2)	Mn(1)−N(3)−O(9)−Mn(2)	50.6(3)
Mn(2)−O(9)	1.982(2)	Mn(2)−O(12)−N(4)−Mn(3)	47.1(3)
Mn(2)−O(12)	1.929(2)	Mn(2)−O(15)−N(5)−Mn(3)	48.7(3)
Mn(2)−O(15)	1.991(2)	Mn(2)−O(18)−N(6)−Mn(3)	47.5(3)

characteristic of Mn^{III} ions. It is noteworthy that the redox properties of the central Mn metal ion toward the +3 state are certainly favored by the ligand choice. Additionally, this +3 oxidation state may have also been facilitated by the intramolecular hydrogen bonds, which help by stabilizing the axially elongated Mn2−O3 and Mn2−O18 bonds as illustrated in Figure 4. For **1** and **2**, the octahedral Mn centers are

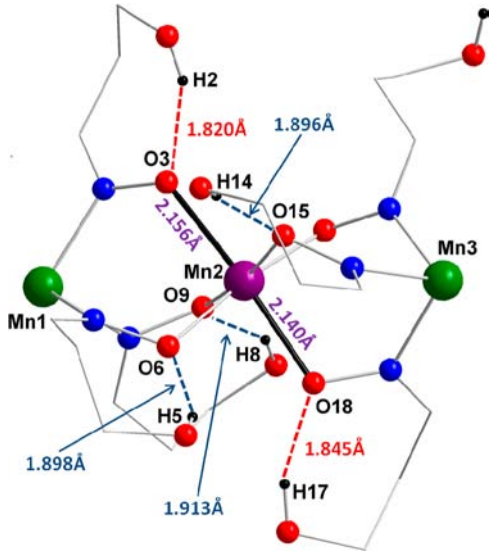

Figure 4. Molecular structure of the trinuclear unit in **2** illustrating the intramolecular hydrogen bonding as well as the J−T axis on Mn2 (central Mn^{III} ion) in black. The shorter H bonds are indicated in red and involve the participation of O3 and O18, which form the J−T axis. Color code: green (Mn^{IV}), purple (Mn^{III}), red (O), blue (N), gray (C).

arranged in a linear or quasi-linear fashion, respectively, where the metal ions are bridged exclusively by six dpo^{2-} ligands for **1** and six $Hoxol^{2-}$ ligands for **2** (Figure 2). Furthermore, the central metal ion (Mn2) is coordinated to six oxygen atoms while the peripheral Mn ions (Mn(1) and Mn(1a) for **1**; Mn(1) and Mn(3) for **2**) are coordinated to three nitrogen atoms and three oxygen atoms. Selected bond distances and angles are presented in Table 2. In **1**, the average Mn(1)−O, Mn(2)−O, and Mn(1)−N distances are 1.83, 1.91, and 1.99 Å, respectively, while in **2**, the average Mn(1)/Mn(3)−O, Mn(1)/Mn(3)−N, Mn(2)−$O_{equatorial}$, and Mn(2)−O_{axial} distances are 1.85, 1.98, 1.97, and 2.15 Å, respectively.

Other important distances involve those separating the Mn centers in the compounds. In complex **1**, the Mn(1)···Mn(2) and Mn(1)···Mn(1a) distances of 3.54 and 7.08 Å, respectively, are comparable to those in **2** with Mn(1)···Mn(2), Mn(2)···Mn(3), and Mn(1)···Mn(3) distances being 3.54, 3.53, and 7.07 Å, respectively (Figure 3). The closest interunit distances in **2** are between Mn(1)···Mn(1) through the Na bridges with distances of 5.85 and 5.92 Å for Na(1) and Na(2), respectively, occurring along the chain as opposed to those in **1** that occur between well-isolated complexes with separations of 12.11, 11.58, and 11.37 Å along the *a* axis (Figure 5), *b* axis (Supporting Information, Figure S1), and *c* axis (Supporting Information, Figure S2), respectively. This structural feature renders the magnetic interactions between trinuclear units in **2** more relevant and can potentially influence the magnetic properties of the compound.

The presence of bulky groups on the ligands induces large torsion angles, which in turn influence the nature and strength of magnetic interactions between the metal ions. The average torsion angle between the terminal and the central manganese ions (Mn(1)−N−O−Mn(2)) was calculated to be 51.3° for **1** and 47.8° for **2** for Mn(1)−N−O−Mn(2) and Mn(2)−N−O−Mn(3), which is much higher than for other trinuclear oximate-bridged complexes (0−20°).[11]

dx.doi.org/10.1021/ic301820w | *Inorg. Chem.* 2013, 52, 1296−1303

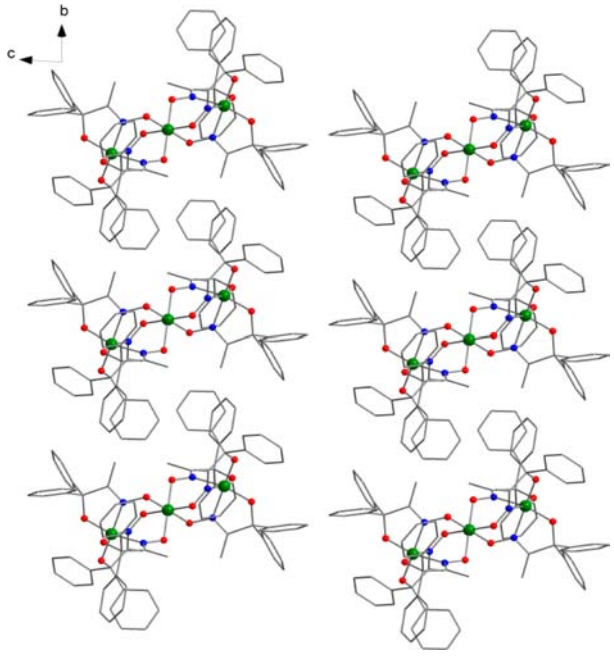

Figure 5. Packing arrangement of **1** along the *a* axis showing well-isolated complexes.

Moreover, the magnetic anisotropy of the $\{Mn_3\}$ system in **2** is derived from a prominent J−T elongation in the axial positions of the central Mn^{III} ions. It is noteworthy that these axial oxygen atoms are participating in intramolecular hydrogen bonds with the nearby protonated hydroxyl groups as illustrated in Figure 4. The oxygen atoms that form the J−T axes on Mn^{III} ions are shown to participate in shorter H bonds than the equatorial oxygen atoms (distances are indicated on the structure in Figure 4). The J−T distortion induces structural and consequently magnetic anisotropy in the system satisfying the second requirement of SMMs and potentially promoting SMM behavior in the trinuclear complex. It is worth mentioning that, to our knowledge, there are only two other previously reported linear trinuclear $\{Mn_3\}$ complexes that behave as SMMs.[12] The packing diagram for **1** along the *a* axis shows well-isolated trinuclear complexes that are organized in a parallel fashion (Figure 5). For **2**, it can be seen from the packing arrangement (Figure 6) that the trinuclear units are linked via Na^+ ions into chains along the *c* axis (this can also be seen in the packing diagrams along the *a* and *b* axes in the Supporting Information, Figures S3 and S4, respectively). The chains are arranged in an antiparallel fashion with the closest interchain distance being 3.44 Å between the two carbon atoms of the dangling ligand arms. The J−T elongations within each chain are aligned parallel to each other; however, they form a 75° angle (noted α thereafter) to neighboring J−T axes in other chains (Figure 6). While the $Mn^{III}\cdots Mn^{IV}$ distance in **2** is comparable to $Mn^{IV}\cdots Mn^{IV}$ distances in **1**, the shortest metal−metal distance between intrachain Mn^{IV} atoms occurs through the sodium ions (5.85 Å for Na(1) and 5.92 Å for Na(2), Figure 3) and is significantly shorter than the distance separating two Mn^{IV} atoms through a Mn^{III} ion (7.08 Å, Figure 3).

Magnetic Properties. The dc magnetic susceptibility measurements for both **1** and **2** were performed between 1.9 and 300 K under an applied dc field of 1000 Oe. The χT versus T plots of **1** and **2** are presented in Figure 7, where the χT

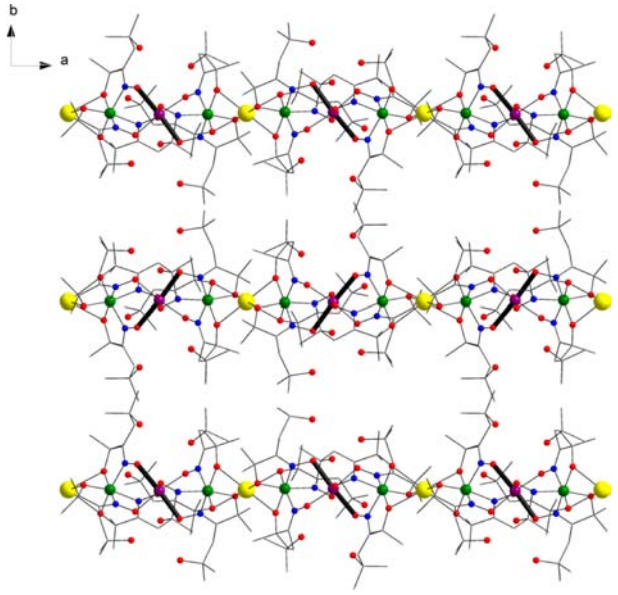

Figure 6. Packing arrangement of **2** along the *c* axis showing chains aligned in an antiparallel fashion highlighting the J−T axes in black.

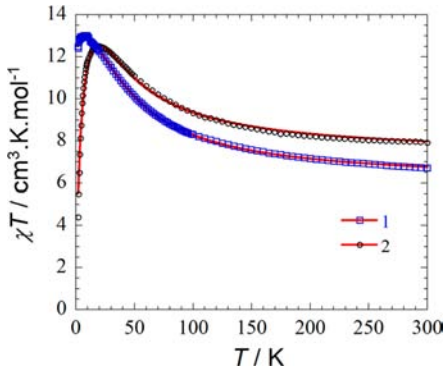

Figure 7. Plot of χT vs T for compounds **1** and **2** at 1000 Oe (with χ defined as molar magnetic susceptibility equal to M/H per mole of complex). The solid lines are the best fits obtained with the Heisenberg trinuclear model (see text).

product at room temperature is 6.7 $cm^3\cdot K\cdot mol^{-1}$ for **1** and 7.2 $cm^3\cdot K\cdot mol^{-1}$ for **2**, which are comparable to the theoretical values (for $g = 2$) of 5.625 $cm^3\cdot K\cdot mol^{-1}$ for **1** and 6.75 $cm^3\cdot K\cdot mol^{-1}$ for **2**. As the temperature decreases, the χT values increase steadily up to 100 K and then rapidly reaching maxima of 13.0 $cm^3\cdot K\cdot mol^{-1}$ at 7.5 K for **1** and 12.5 $cm^3\cdot K\cdot mol^{-1}$ at 19 K for **2** indicating dominant intramolecular ferromagnetic interactions. The maximum value of χT for **1** is in accordance with a spin ground state of $S_T = {}^9/_2$ (theoretical value of 12.375 $cm^3\cdot K\cdot mol^{-1}$ when $g = 2$). For **2**, the maximum of the χT value is slightly lower but also in agreement (vide infra) with the theoretical value (15.0 $cm^3\cdot K\cdot mol^{-1}$ when $g = 2$) expected for an $S_T = 5$ spin ground state.

The final decrease at low temperature of the χT product suggests the presence of intermolecular antiferromagnetic interactions and/or the presence of magnetic anisotropy. It is evident that the main magnetic interactions between the metal centers occur through superexchange pathways formed by the oxime groups from the dpo^{2-} (**1**) and $Hoxol^{2-}$ (**2**) ligands (Figure 2). Fitting of the magnetic susceptibility data for **1** was carried out in order to determine the sign and magnitude of the

dx.doi.org/10.1021/ic301820w | *Inorg. Chem.* 2013, 52, 1296−1303

intramolecular interactions between Mn^{IV} ions. The following Heisenberg Hamiltonian was employed: $H = -2J\{\vec{S}_1\vec{S}_2 + \vec{S}_1\vec{S}_3\}$ where J is the intramolecular magnetic exchange interaction between a terminal Mn^{IV} ion and a central Mn^{IV} ion, $\vec{S}_i$ is the spin operator for each Mn with $S = {}^3/_2$ (Mn^{IV}) as seen in Scheme 2, top. The low field magnetic susceptibility was

Scheme 2. Schematic Diagram Showing the Intra- and Intermolecular Magnetic Interactions between Mn ions in 1 (top) and 2 (bottom)

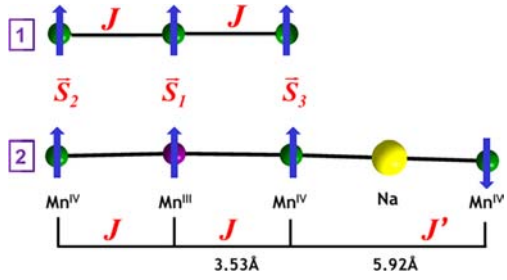

calculated by applying the van Vleck equation[13] to Kambe's vector coupling scheme,[14] and the experimental data were fitted yielding the following parameters: $J/k_B = +11.5(1)$ K, $g = 2.06(3)$, and $J'/k_B = -0.06(1)$ K; where J' is the intercomplex magnetic interaction introduced in the frame of the mean field theory.[10,11] This data indicates ferromagnetic interactions between metal centers and thus a spin ground state of $S_T = {}^9/_2$ with the first ($S = {}^7/_2$) and second ($S = {}^5/_2$) excited states being 34.2 and 69.7 K higher in energy, respectively.[10] For such linear, triply bridged oxime systems with torsion angles such as in **1** and **2**, ferromagnetic interactions between metal centers and thus high-spin ground states are commonly observed.[15] The field dependence of the magnetization plot at varying temperatures for **1** is shown in Figure S5 of the Supporting Information. The clear saturation of the curve at 1.8 K indicates the absence of magnetic anisotropy, with a saturation value of 9.6 μ_B confirming a spin ground state of $S_T = {}^9/_2$. The M versus H/T data was also fitted to a Brillouin function with $S_T = {}^9/_2$ and $g = 2.11(3)$ further confirming the lack of anisotropy. This was expected as all three Mn ions in **1** are in the +4 oxidation state that is known to be isotropic preventing the complex from behaving as an SMM.

For **2**, the same Heisenberg Hamiltonian was employed with the following modifications: J is the intramolecular magnetic exchange interaction now between Mn^{IV} and Mn^{III} ions while the intercomplex magnetic interaction, J', is dominated by the Mn^{IV}–Mn^{IV} interaction via sodium cations (Scheme 2), $\vec{S}_i$ is the spin operator for each Mn with $S_1 = 2$ (Mn^{III}) and $S_2 = S_3 = {}^3/_2$ (Mn^{IV}) as seen in Scheme 2, bottom. The best fit to the experimental data yielded the following parameters: $J/k_B = +7.1(2)$ K, $g = 2.07(3)$, and $J'/k_B = -0.09(2)$ K. In comparison to that of **1**, it is evident that the antiferromagnetic intermolecular interaction is stronger in **2** which explains the somewhat low χT value at 19 K relative to the theoretical $S_T = 5$ value. It should be noted that the J' value should be taken with caution as it also contains phenomenologically the contribution from the magnetic anisotropy. By using the calculated J value, the energies of the excited states were determined resulting in a spin ground state of $S_T = 5$ with the first ($S = 4$) and second ($S = 3$) excited states being 27.3 and 54.9 K higher in energy, respectively.

The M versus H and M versus H/T plots for **2** (Figure 8) show nonsaturation of the magnetization at low temperature and high field (1.9 K and 7 T) as well as nonsuperposition of the curves on a single master curve indicating the presence of magnetic anisotropy. Attempts to fit this data with an $S_T = 5$ macro-spin approximation ($H = DS_{T,z}^2 + E(S_{T,x}^2 - S_{T,y}^2)$) using the program Magnet[16] were fruitless as intermolecular exchange interactions are present between trinuclear units. The signature of these intercomplex interactions along the chain is indeed very clear in the M versus H data at 1.9 K that display a typical "S" shape below 1.0 T (Figure 8).

In order to investigate the effect of added anisotropy to the system through the presence of Mn^{III} ions in **2**, ac magnetic susceptibility measurements were performed in the temperature range 1.8–5 K and frequency range 10–1500 Hz. The out-of-phase susceptibility χ'' versus T plot is shown in Figure 9, top (χ' vs T plot is shown in the inset), and displays a tail of a relaxation peak evident at low temperature. This feature is indicative of slow relaxation of the magnetization and thus of potential SMM behavior that is absent in the parent $\{Mn^{IV}{}_3\}$ compound **1**. This difference of properties can be directly attributed to the anisotropy introduced by the Mn^{III} ions in **2**. In order to confirm this behavior, single-crystal dc magnetization measurements were carried out on a micro-SQUID apparatus[17] at temperatures below 5 K (Figure 9, bottom, and Supporting Information, Figure S6). At temperatures below 1 K for an applied dc field oriented in the easy magnetic direction of a single crystal, M versus H hysteresis loops are observed that

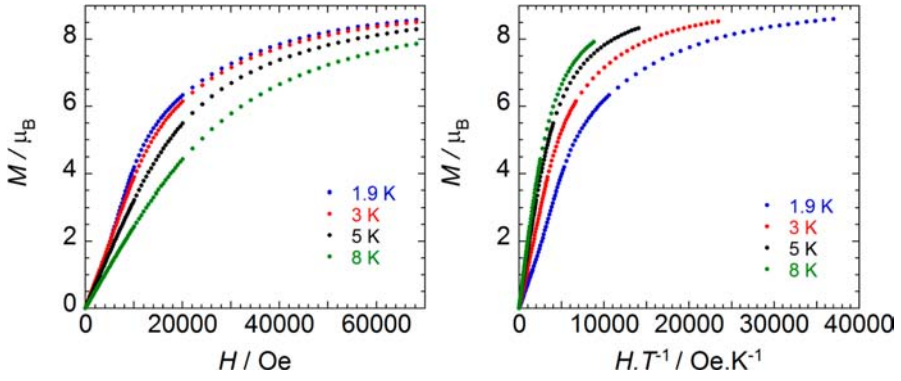

Figure 8. Magnetization vs field measurements at 1.9, 3, 5, and 8 K for a polycrystalline sample of **2** plotted as M vs H (left) and M vs H/T (right). The nonsaturation of the magnetization curves at high fields indicates the presence of magnetic anisotropy in the system. The "S" shape M vs H plot highlights the presence of weak antiferromagnetic interactions between trinuclear complexes.

dx.doi.org/10.1021/ic301820w | Inorg. Chem. 2013, 52, 1296–1303

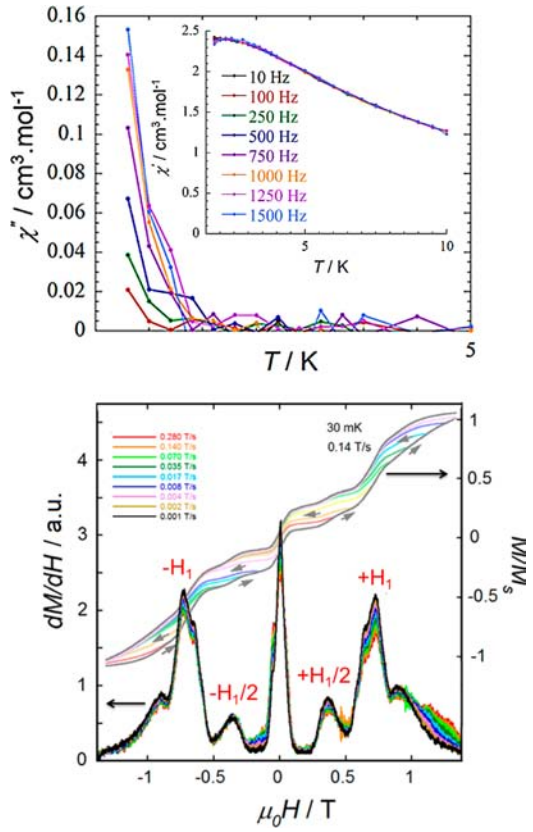

Figure 9. (top) Temperature dependence of the out-of-phase ac magnetic susceptibility plotted as χ'' vs T for **2** in zero applied dc field with an ac oscillating field of 3 Oe at the indicated frequencies; inset shows the corresponding in-phase susceptibility, χ', vs T for **2**. (bottom) Plot of M/M_s and dM/dH vs H obtained from oriented single-crystal (in the easy magnetic direction) measurements at 30 mK and a field sweep rate of 0.14 T/s for compound **2**.

confirm the slow relaxation of the magnetization detected in **2** by ac susceptibility (Figure 9, top). There are three major steps in the M/M_s versus H plot at $H = 0$ and ± 0.73 T ($\pm H_1$ in Figure 9, bottom) that are better seen on the dM/dH versus H plot. This type of behavior has been previously described in detail[18] and is typical of a chain of weakly antiferromagnetically coupled SMMs. Therefore, in order to understand the M/M_s versus H behavior of **2** shown in Figure 9, bottom, the whole chain as trinuclear SMM units interacting through Na bridges must be considered. When a strong negative dc field is applied, the $\{Mn_3\}$ magnetic moments are all aligned along the direction of the applied field. As the applied field reaches $\pm H_1$ corresponding to the intrachain exchange, the spins of the trinuclear unit experience an effective zero field and can therefore flip by quantum tunneling of the magnetization (QTM). Between $H = -H_1$ and $+H_1$, the intrachain magnetic interactions are dominating, but some of the trinuclear unit moments in the chain are trapped in a state where they are not regularly antiparallel, creating magnetic defects (in an effective zero exchange field) along the chain. The minor steps observed at $H = \pm 0.36$ T, which are labeled as $\pm H_1/2$, correspond to the expected quantum relaxation seen for open-ended chains of a finite size where the last spin flips.[18] From the H_1 value, the intrachain interactions, J', can be estimated equalizing the Zeeman and exchange energies: $g\mu_B H_{eff} S_T = 4|J'|S_T^2$.[18] As the measurements have been performed in the easy direction of the crystal (found along the b axis, i.e., at an $\alpha/2$ angle from the J–T axes of the two different chains, Figure 6), the two symmetry related chains experience the same effective dc field: $H_{eff} = H \cos(\alpha/2)$. Therefore J'/k_B is accurately estimated at $-0.039(5)$ K, in good agreement with the rough mean-field value estimated from the χT versus T fit (vide supra).

The absence of full peaks with maxima in the χ'' versus T plot above 1.8 K and the complicated exchange-bias relaxation see in Figure 9 prevent the estimation of the SMM energy barrier. It is noteworthy that performing the ac measurements under a weak dc field above 1.8 K did not shortcut the QTM significantly to allow the observation of the maximum of the frequency-dependent ac peaks.

CONCLUSION

Through careful synthetic strategy, two analogous linear $\{Mn_3\}$ compounds were isolated with high-spin ground states and very different magnetic properties. In both compounds, the metal centers are coupled ferromagnetically through triple-oxime superexchange pathways yielding $S_T = {}^9/_2$ and $S_T = 5$ high-spin compounds. By employing the oxol ligand, we were able to promote the formation and isolation of a previously predicted yet elusive Mn^{IV}–Mn^{III}–Mn^{IV} unit. The incorporation of Mn^{III} ions into the system introduces magnetic anisotropy that subsequently "turns on" the SMM behavior. The latter strategy provides a new avenue/methodology to fine-tuning a simple system in order to control the switching on of their magnet-like behavior.

ASSOCIATED CONTENT

Supporting Information

Crystallographic data (including CIF file), packing diagrams, and additional magnetic measurement plots of **1** and **2**. This material is available free of charge via the Internet at http://pubs.acs.org.

AUTHOR INFORMATION

Corresponding Author

*Phone: +33 5 56 84 56 50 (R.C.), 613-562-5800 ext 2733 (M.M.). Fax: +33 5 56 84 56 00 (R.C.), 613-562-5170 (M.M.). E-mail: clerac@crpp-bordeaux.cnrs.fr (R.C.), m.murugesu@uottawa.ca (M.M.).

Author Contributions

The manuscript was written through contributions of all authors. All authors have given approval to the final version of the manuscript.

Notes

The authors declare no competing financial interest.

ACKNOWLEDGMENTS

We thank the University of Ottawa, the Canada Foundation for Innovation (CFI), FFCR, NSERC (Discovery and RTI grants), the Conseil Régional d'Aquitaine, GIS Advanced Materials in Aquitaine (COMET Project), the Université de Bordeaux, the CNRS, and the ANR (NT09_469563, AC-MAGnets project) for financial support. We also thank Dr. Ilia Korobkov (University of Ottawa) and Francine Bélanger-Gariépy (Université de Montréal) for their help with the single-crystal X-ray crystallography.

REFERENCES

(1) (a) Zaleski, C. M.; Depperman, E. C.; Kampf, J. W.; Kirk, M. L.; Pecoraro, V. L. *Angew. Chem., Int. Ed.* **2004**, *43*, 3912. (b) Milios, C. J.; Vinslava, A.; Whittaker, A. G.; Parsons, S.; Wernsdorfer, W.; Christou, G.; Perlepes, S. P.; Brechin, E. K. *Inorg. Chem.* **2006**, *45*, 5272. (c) Milios, C. J.; Inglis, R.; Vinslava, A.; Bagai, R.; Wernsdorfer, W.; Parsons, S.; Perlepes, S. P.; Christou, G.; Brechin, E. K. *J. Am. Chem. Soc.* **2007**, *129*, 12505.

(2) Milios, C. J.; Inglis, R.; Bagai, R.; Wernsdorfer, W.; Collins, A.; Moggach, S.; Parsons, S.; Perlepes, S. P.; Christou, G.; Brechin, E. K. *Chem. Commun.* **2007**, 3476.

(3) (a) Ferbinteanu, M.; Miyasaka, H.; Wernsdorfer, W.; Nakata, K.; Sugiura, K.-i.; Yamashita, M.; Coulon, C.; Clérac, R. *J. Am. Chem. Soc.* **2005**, *127*, 3090. (b) Scott, R. T. W.; Parsons, S.; Murugesu, M.; Wernsdorfer, W.; Christou, G.; Brechin, E. K. *Angew. Chem., Int. Ed.* **2005**, *44*, 6540. (c) Wang, W.-G.; Zhou, A.-J.; Zhang, W.-X.; Tong, M.-L.; Chen, X.-M.; Nakano, M.; Beedle, C. C.; Hendrickson, D. N. *J. Am. Chem. Soc.* **2007**, *129*, 1014.

(4) (a) Christou, G.; Gatteschi, D.; Hendrickson, D. N.; Sessoli, R. *MRS Bull.* **2000**, *25*, 66. (b) Aromi, G.; Brechin, E. K. *Struct. Bonding (Berlin, Ger.)* **2006**, *122*, 1.

(5) Milios, C. J.; Vinslava, A.; Wernsdorfer, W.; Moggach, S.; Parsons, S.; Perlepes, S. P.; Christou, G.; Brechin, E. K. *J. Am. Chem. Soc.* **2007**, *129*, 2754.

(6) (a) Sessoli, R.; Powell, A. K. *Chem. Rev.* **2009**, *253*, 2328 (and references therein). (b) Hołynska, M.; Premuzic, D.; Jeon, I.-R.; Wernsdorfer, W.; Clérac, R.; Dehnen, S. *Chem.—Eur. J.* **2011**, *17*, 9605.

(7) Stamatatos, T. C.; Teat, S. J.; Wernsdorfer, W.; Christou, G. *Angew. Chem., Int. Ed.* **2009**, *48*, 521.

(8) Glaser, T. *Chem. Commun.* **2011**, *47*, 116 (and references therein).

(9) (a) Zaleski, C. M.; Weng, T.-C.; Dendrinou-Samara, C.; Alexiou, M.; Kanakaraki, P.; Hsieh, W.-Y.; Kampf, J.; Penner-Hahn, J. E.; Pecoraro, V. L.; Kessissoglou, D. P. *Inorg. Chem.* **2008**, *47*, 6127. (b) Mukhopadhyay, S.; Armstrong, W. H. *J. Am. Chem. Soc.* **2003**, *125*, 13010.

(10) Pathmalingam, T.; Gorelsky, S. I.; Burchell, T. J.; Bédard, A.-C.; Beauchemin, A. M.; Clérac, R.; Murugesu, M. *Chem. Commun.* **2008**, 2782.

(11) (a) Price, D. J.; Batten, S. R.; Berry, K. J.; Moubaraki, B.; Murray, K. S. *Polyhedron* **2003**, *22*, 165. (b) Johnson, B. F. G.; Sieker, A.; Blake, A. J.; Winpenny, R. E. P. *J. Chem. Soc., Chem. Commun.* **1993**, 1345. (c) Birkelbach, F.; Florke, U.; Haupt, H. J.; Butzlaff, C.; Trautwein, A. X.; Wieghardt, K.; Chaudhuri, P. *Inorg. Chem.* **1998**, *37*, 2000.

(12) (a) Scott, R. T. W.; Parsons, S.; Murugesu, M.; Wernsdorfer, W.; Christou, G.; Brechin, E. K. *Chem. Commun.* **2005**, 2083. (b) Zhou, C.-L.; Wang, Z.-M.; Wang, B.-W.; Gao, S. *Dalton Trans.* **2012**, *41*, 13620.

(13) van Vleck, J. H. *The Theory of Electric and Magnetic Susceptibility*; Oxford University Press: Oxford, U.K., 1932.

(14) Kambe, K. *J. Phys. Soc. Jpn.* **1950**, *5*, 48.

(15) (a) Birkelbach, F.; Flörke, U.; Haupt, H.-J.; Butzlaff, C.; Trautwein, A. X.; Wieghardt, K.; Chaudhuri, P. *Inorg. Chem.* **1998**, *37*, 2000. (b) Alexiou, M.; Dendrinou-Samara, C.; Karagianni, A.; Biswas, S.; Zaleski, C. M.; Kampf, J.; Yoder, D.; Penner-Hahn, J. E.; Pecoraro, V. L.; Kessissoglou, D. P. *Inorg. Chem.* **2003**, *42*, 2185. (c) Price, D. J.; Batten, S. R.; Moubaraki, B.; Murray, K. S. *Polyhedron* **2003**, *22*, 165. (d) Audhya, A.; Maity, M.; Abtab, S. M. T.; Mathonière, C.; Kalisz, M.; Clérac, R. *Polyhedron* **2012**, *33*, 353. (e) Mukherjee, C.; Weyhermüller, T.; Wieghardt, K.; Chaudhuri, P. *Dalton Trans.* **2006**, 2169. (f) Pavlishchuk, V.; Birkelbach, F.; Weyhermüller, T.; Wieghardt, K.; Chaudhuri, P. *Inorg. Chem.* **2002**, *41*, 4405.

(16) Davidson, E. R. *Magnet*; Indiana University: Bloomington, IN, 1999.

(17) Wernsdorfer, W. *Supercond. Sci. Technol.* **2009**, *22*, 064013.

(18) Lecren, L.; Wernsdorfer, W.; Li, Y.-G.; Vindigni, A.; Miyasaka, H.; Clérac, R. *J. Am. Chem. Soc.* **2007**, *129*, 5045.

(19) (a) *SHELXTL*, v. 6.12; Bruker Analytical X-ray Systems Inc.: Madison, WI, 2001; pp 53719−1173. (b) Sheldrick, G. M. *Acta Crystallogr.* **2008**, *A64*, 112.